A Novel Model for Interferometric Phase Reconstruction Based on Multi-Stage Conditional GANs

Mahmoud Abdallah[1, 2, 3], Xiaoli Ding[1, 2], Songbo Wu[1, 2]

[1] Department of Land Surveying and Geo-Informatics, The Hong Kong Polytechnic University, Hong Kong, China - mahmoud.abdallah@connect.polyu.hk, xl.ding@polyu.edu.hk, songbo.wu@connect.polyu.hk
[2] Research Institution for Land and Space, The Hong Kong Polytechnic University, Hong Kong, China
[3] Public Works Department, Mansoura University, Mansoura, Egypt

Keywords: InSAR; phase reconstruction; generative adversarial networks (GANs); decorrelation region.

Abstract

Reconstructing the interferometric phase in decorrelated regions is a significant challenge in interferometric synthetic aperture radar (InSAR) techniques, as decorrelation disrupts the continuity of phase fringes and obscures critical information. This paper presents a novel two-stage generative adversarial network (GAN) framework to address this issue. In the first stage, GAN is designed to reconnect fragmented phase fringes. In the second stage, GAN focuses on reconstructing the phase in masked regions guided by the reconnected fringes achieved from the first stage. The proposed model was trained on a simulated topographic phase with the SRTAM product. The proposed model achieves a structural similarity index (SSIM) of 0.9 and a peak signal-to-noise ratio (PSNR) of 30.4. Then, we conducted a quantitative evaluation with a real interferogram from the Greater Bay Area (GBA). The experiment results demonstrated the generalization capabilities of the proposal model, with an average correlation of 0.8 between the predicted and actual phases. The proposed approach can effectively preserve phase continuity, reconstruct masked areas, and mitigate the impact of decorrelation. It shows potential for use in topographic retrieval and ground deformation monitoring in InSAR applications.

1. Introduction

Phase decorrelation is one of the significant challenges in Interferometric Synthetic Aperture Radar (InSAR) applications, particularly over the vegetated regions (Hanssen, 2001; Lee and Liu, 2001; Abdallah et al., 2024a). InSAR relies on phase differences, characterized by high phase quality and coherence, between successive radar acquisitions to measure surface deformation (Zebker and Villasenor, 1992). However, in areas with steep terrain, denser vegetation, or rapid surface changes, the phase coherence is often reduced, leading to phase decorrelation (Gavas et al., 2023). This reduction can result in incomplete or noisy data, hindering the accuracy of InSAR measurements.

Traditional phase filtering techniques are commonly used to mitigate decorrelation effects. For instance, the Goldstein filter, one of the most widely adopted algorithms for noise reduction before phase unwrapping, applies a spectral filter to remove high-frequency noise while preserving essential phase fringes for accurate unwrapped phase estimation (Goldstein and Werner, 1998). Although effective in many scenarios, such methods often struggle in cases of severe decorrelation, particularly in areas with steep terrain or dense vegetation (Gavas et al., 2023). An alternative approach is the use of masking to exclude decorrelated regions; however, this can be time-consuming and requires expert input to accurately identify affected areas (Zhang et al., 2021). Unresolved masked areas lead to spatially incomplete InSAR results, resulting in the loss of critical information for applications such as topographic construction.

Spatial interpolation methods, such as Kriging, offer a potential solution for reconstructing the phase over the decorrelation regions (Wu et al., 2013). Despite their effectiveness, these methods often face challenges with significant gaps or wrapped phase (Hippert-Ferrer et al., 2021). Additionally, statistical methods were explored for phase reconstruction, but they can be sensitive to the strength and quality of the recorded signals (Prebet et al., 2019).

Recent advancements in deep learning (DL) have significantly transformed the field of InSAR such as deformation retrieval and interpretation (Abdallah et al., 2024b, 2025). In particular, generative adversarial networks (GANs) (Goodfellow et al., 2014) have introduced innovative approaches for phase reconstruction in InSAR (Abdallah et al., 2024a). GANs comprise two neural networks—a generator and a discriminator—trained in an adversarial manner. The generator is designed to create realistic reconstructed outputs, while the discriminator evaluates their quality and provides feedback to enhance the performance of the generator in producing accurate reconstructions (Goodfellow et al., 2014). GANs have been used in various InSAR applications, including phase denoising (Fang et al., 2022), phase unwrapping (Zhou et al., 2022), atmospheric artifact removal (Rongier et al., 2020), simulating InSAR signals (Zhou et al., 2024), and generating realistic interferograms (Chen et al., 2021).

Numerous GAN variants have also been explored. For instance, conditional GANs (cGANs) use extra information to guide both the generator and discriminator, allowing for more controlled generation (Isola et al., 2017; Nazeri et al., 2019). It has been proven particularly effective in image translation tasks, transforming images from one domain to another while maintaining contextual relevance by conditioning on input images (Isola et al., 2017). PatchGAN further improves image quality by focusing on local patches rather than the entire image, thereby capturing high-frequency details for sharper, more realistic outputs (Isola et al., 2017). Multi-stage GANs, which break down tasks into subtasks, with each GAN addressing a specific aspect, have shown impressive results in image translation, reconstruction, and inpainting tasks (Nazeri et al., 2019). In the context of InSAR, the phase reconstruction procedure can be divided into two stages: fringe reconnection and phase reconstruction. Reconnecting the fringes based on remaining contextual information allows for a more accurate interpretation of the interferometric phase in decorrelated regions (Abdallah et al., 2024a). Thus, multi-stage GANs are well-suited to address these challenges.

In this work, we propose a novel two-stage GAN framework to reconnect phase fringes and reconstruct the phase over masked regions caused by decorrelation in a unified approach. The framework consists of two distinct GAN models with the same generator and a conditional PatchGAN discriminator. The first GAN, the Fringe Reconnector Network (FRN), focuses on reconnecting fragmented phase fringes disrupted by decorrelation. Once the fringes are restored, the second GAN, the Phase Reconstructor Network (PRN), reconstructs the phase in masked regions, leveraging the reconnected fringes as contextual information. It is worth noting that the choice of loss functions, such as pixel-level losses (L1 or L2 norms) and feature-level losses (perceptual loss), is critical for training GANs for image synthesis, with perceptual loss being especially effective in capturing higher-level perceptual differences for visually appealing results (Nazeri et al., 2019). In this regard, we designed a combined loss to enhance overall phase reconstruction and provide a more accurate interpretation of the InSAR interferometric phase. The proposed model is trained using simulated data and verified through real experiments. The results indicate the effectiveness of the model in phase reconstruction over decorrelation regions and demonstrate its generalization capabilities in different scenarios.

The following sections of this paper are organized as follows: Section 2 provides an overview of the materials and methods, detailing the model architecture, data preparation process, and training methodologies. Section 3 analyzes and discusses the results obtained from the experiments. The paper concludes with Section 4, which summarizes the main findings and proposes potential avenues for future research.

2. Material and Methods

This section outlines the model architecture, dataset, preprocessing steps, and training process used in our proposed two-stage GAN framework for phase reconstruction over decorrelated topography. The model was trained and tested on an interferometric dataset derived from two regions in China.

2.1 Model architecture

The proposed approach employs a two-stage generative adversarial network (GAN) framework for phase reconstruction. The overall architecture of the two-stage GAN model is illustrated in Figure 1. The first stage focuses on fringe reconnection, and the second stage addresses masked region reconstruction, utilizing the reconnected fringes as contextual information. Each GAN comprises a generator and a discriminator and is trained in an adversarial setting.

In the Fringe Reconnector Network (FRN), the generator receives sliced patches, including masked interferogram, masked fringes, and the corresponding mask patches, and learns to reconnect fragmented phase fringes caused by decorrelation (i.e., Figure 1 (a)). The discriminator evaluates the authenticity of the reconnected fringes by determining whether they are realistic or remain disconnected, using the ground-truth interferogram as a reference. Once the fringes are reconnected, the second stage, known as the Phase Reconstructor Network (PRN), focuses on reconstructing the phase in the masked regions (i.e., Figure 1 (b)). The generator in this stage is guided by the reconnected fringes from the FRN, ensuring that the reconstructed phase aligns consistently with the surrounding interferogram.

Both GANs share the same generator and discriminator architecture. The generator follows an encoder-decoder design, where the encoder downsamples the input patches twice. This is followed by eight residual blocks, which capture fine-grained details while preserving global context and ensuring smooth gradient flow across all layers. The decoder then upsamples the patches back to their original size. The discriminator, leveraging a PatchGAN, classifies 70 × 70 pixel segments of the generated phase as either real or fake.

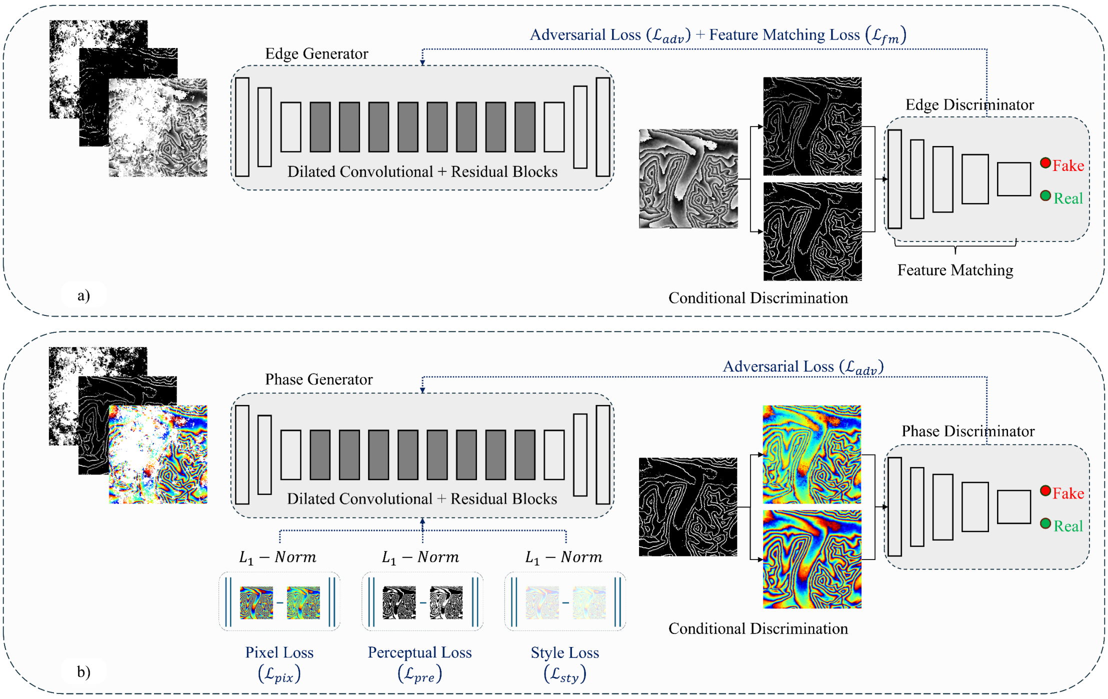

Figure 1. The proposed architecture for the interferometric phase reconstruction (IPR). a) The fringe reconnector network (FRN). b) The phase reconstructor network (PRN).

2.2 Dataset

We trained the proposed model using a simulated InSAR dataset. The SRTM product is used to generate the topographic phase, located at 27°–29° Easting and 85°–88° Northing, as shown in Figure 2 (a). The simulated interferometric phase was computed using Equation (1) and wrapped to a value of 2π, as depicted in Figure 2 (b). A decorrelation mask was generated using a random function to create a coherence map, and a threshold of 0.5 was applied, resulting in approximately 50% of the pixels being masked, as shown in Figure 2 (d).

$$\varphi(i,j) = \mathrm{mod}\left(\frac{4\pi * B_{\perp} * h_{(i,j)}}{\lambda * R * \sin(\theta)}, 2\pi\right) \tag{1}$$

where $\varphi(i,j)$ is the wrapped phase of the pixel (i,j), $B_{\perp}$ is the perpendicular baseline, set to 100.0 m, λ is the radar wavelength (0.055 m), R is the orbit height (907 km), θ is the incidence angle (42.1°), $h_{(i,j)}$ is the altitude, obtained from the three arc-second SRTM DEM dataset.

2.3 Preprocessing

To prepare the data for the GAN models, we sliced the interferogram and the corresponding mask into smaller overlapping patches, each of size 256 × 256 pixels. A stride of 128 pixels was used to ensure overlapping and capture contextual information between patches. This sliding window approach ensures that each patch shares information with its neighbors, both horizontally and vertically. Figure 2 (c) and (e) show examples of the interferogram and mask patches, respectively. The interferogram patches were normalized to the range of [0, 1] for input into the FRN. In contrast, they were normalized to the range [-1, 1] for the PRN to maintain data consistency across the stages. Fringe lines were identified from one of the initial feature maps of the VGG-19 model, which was pre-trained on the ImageNet dataset (Russakovsky et al., 2015; Simonyan and Zisserman, 2015). A threshold of 0.5 was applied to extract these lines, reinforcing the concept that the earlier layers in a deep convolutional neural network (CNN) function as edge detectors (Le and Kayal, 2021).

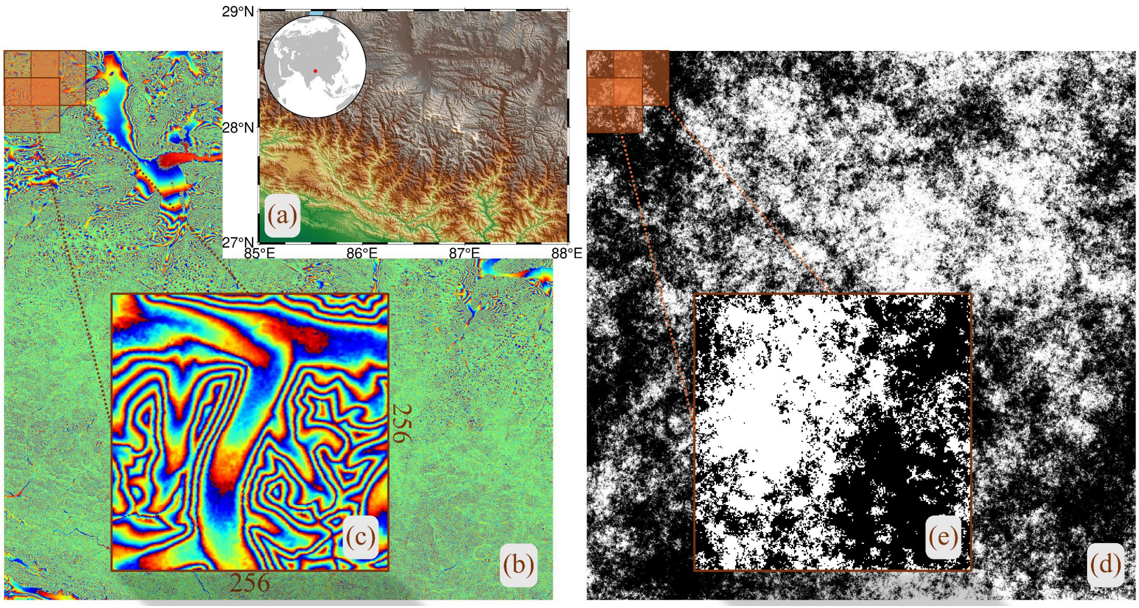

Figure 2. The simulated data used for training the network. a) The geographic location of the SRTM used to generate the topographic phase. b) The simulated interferogram. c) The extracted patch from the interferogram. d) The simulated decorrelation mask. e) The extracted patch from the decorrelation mask. The patch size equals 256 × 256 pixels with a stride of 128 pixels.

2.4 Loss function

To optimize the two-stage GAN model, we employed a combination of reconstruction and adversarial losses. The adversarial loss encourages the generator to produce realistic interferometric phase reconstructions, while the reconstruction loss ensures that the reconnected fringes and masked regions align with the true phase values. The overall loss function for both GANs is defined as follows:

$$\min_G \max_D \mathcal{L} = \min_G \left(\lambda_{adv} \max_D \mathcal{L}_{adv} + \lambda_{recon}\mathcal{L}_{recon}\right) \tag{2}$$

where $\mathcal{L}_{adv}$ represents the adversarial loss, $\mathcal{L}_{recon}$ is the reconstruction loss, and λ_{adv} and λ_{recon} are weighting factors that balance the two losses. In the FRN, the reconstruction loss is a feature-matching loss derived from the discriminator, whereas in the PRN, it is a weighted combination of pixel and feature space losses.

2.5 Training and Evaluation

The model was trained using a simulated dataset including topographic phase component, which was divided into an 80% training set and a 20% validation set. Initially, the two GANs were trained independently with a learning rate of 10^{-5}, followed by joint training at a reduced learning rate of 10^{-5} until convergence was achieved. The Adam optimizer was utilized to iteratively optimize both the generator and the discriminator (Kingma and Ba, 2015). During training, the generator minimized the adversarial and reconstruction losses, and the discriminator distinguished between real and generated phase reconstructions.

To evaluate the performance of the model, we compared the reconstructed phase data with the simulated truth, focusing mainly on decorrelation regions. Evaluation metrics included accuracy, precision, and recall assessing fringe reconnection quality. Furthermore, the accuracy of the phase reconstruction is assessed through several metrics, including mean squared error (MSE), mean absolute error (MAE), peak signal-to-noise ratio (PSNR), and structural similarity index (SSIM).

3. Results and discussions

This section presents the results of the proposed two-stage GAN framework for phase reconstruction over decorrelated regions. The results include both qualitative visualizations of phase reconnection and reconstruction, as well as quantitative metrics that assess the accuracy and consistency of the reconstructed phases.

3.1 Phase Reconnection

The first stage of our framework is focused on reconnecting phase fringes in areas where decorrelation has disrupted the continuity of phase patterns. Figure 3 provides a side-by-side comparison of the input fragmented phase fringes (2nd column), which exhibit visible discontinuities, with the output reconnected fringes (3rd column) that show smoother transitions and fewer breaks in continuity. The ground truth fringe lines are displayed in the 4th column. The FRN effectively preserves the overall structure of the fringes while reconnecting broken segments, establishing a robust foundation for the subsequent phase reconstruction.

Initially, the FRN generator assumes all masked pixels are positive. Through multiple iterations, the model learns to remove low-probability pixels, ultimately producing complete fringe lines. To quantify the effectiveness of this approach, we evaluate the reconstructed interferograms using reconnection metrics. As shown in Table 1, the model achieves high accuracy, precision, and recall, indicating that the reconnected fringes are structurally consistent with the ground truth in both the training and validation datasets.

Data	Accuracy	Precision	Recall
Training	0.9230	0.8424	0.6853
Validation	0.9197	0.8369	0.6887

Table 1. Summary of Accuracy, Precession, and Recall scores for training and validation datasets used for FRN.

3.2 Phase Reconstruction

The PRN reconstructs the phase over masked regions, leveraging the output of the FRN as contextual information. Initially, the FRN was trained using ground truth fringe lines to familiarize the model with the general characteristics of the interferometric phase. As shown in Table 2, reconstruction using the PRN with ground truth fringes achieves state-of-the-art results. In the second step, the reconnected fringes are input to the trained PRN to adapt the model to actual fringe patterns. Figure 3 provides examples of the input-masked interferograms (1st column), the corresponding outputs after phase reconstruction (5th column), and the ground truth interferograms (6th column). The model demonstrates impressive performance in reconstructing interferograms, even when the reconnected fringes are incomplete (as seen in the 1st row). This performance is achieved after fine-tuning both models in a unified step.

To quantify the effectiveness of this approach, we evaluate the reconstructed interferograms using reconstruction metrics. As shown in Table 2, the model achieves low mean MAE and MSE, as well as high SSIM and PSNR, indicating that the reconstructed phase is accurate and structurally consistent with the ground truth. The slight performance degradation is attributed to incomplete fringes in large, masked regions.

The PRN focuses on reconstructing the phase over masked regions, using the output of the first GAN as contextual information. Firstly, we train the FRN network using the ground truth fringe lines to teach the model of the general characteristics of the interferometric phase. Table 2 shows that the reconstruction using the PRN with ground truth fringes achieves state-of-the-art results. The second step is to submit the reconstructed fringes to the trained PRN network to adapt the model to the actual fringes. Figure 3 shows examples of input-masked interferograms (1st column), the corresponding outputs after phase reconstruction (5th column), and the ground-truths interferogram (6th column).

To quantify the effectiveness of our approach, we evaluate the reconstructed interferograms using reconstruction metrics. As shown in Table 2, the model achieves a low MAE and MSE and high SSIM and PSNR on the training and validation, indicating that the reconstructed phase is accurate and structurally consistent with the ground truth. The slight degradation in the model performance is related to the incomplete fringes that may arise in large, masked regions.

Edge	Data	MAE	MSE	SSIM	PSNR
Ground -truth	Training	0.0100	0.0003	0.9864	41.1115
	Validation	0.0101	0.0003	0.9861	41.3182
Reconstructed	Training	0.0198	0.0037	0.9034	30.4032
	Validation	0.0198	0.0037	0.9033	30.4031

Table 2. Summary of the MAE, MSE, SSIM, and PSNR scores for training and validation datasets used for PRN.

3.3 Two-stage GAN

To assess the contribution of each stage in the GAN framework, we conducted an experiment evaluating the performance of the model when using the PRN without the support of fringe reconnection, effectively creating a one-stage solution. As shown in Table 3, the two-stage GAN framework outperforms the single-stage GAN by 8% in SSIM and 36% in PSNR. These results underscore the significance of dividing the interferometric phase reconstruction task into simpler subtasks, demonstrating that fringe reconnection substantially enhances the overall performance. Future improvements to the FRN will likely further push the framework towards state-of-the-art results.

Edge	MAE	MSE	SSIM	PSNR
Ground-truth	0.0101	0.0003	0.9861	41.3182
Reconnected	0.0198	0.0037	0.9033	30.4031
Without	0.0256	0.0076	0.8256	22.1257

Table 3. Summary of MAE, MSE, SSIM, and PSNR scores for different edge configurations used in the PRN.

3.4 Generalization to Unseen Data

One of the primary challenges in deep learning is ensuring that trained models can generalize effectively to unseen data. In our experiments, the test region in the Greater Bay Area (GBA) served as a meaningful case study to evaluate the robustness of our model. The results suggest that the two-stage GAN framework generalizes well to different terrains with similar decorrelation patterns. Figure 4 (a) shows the geographic location of the study area while Figure 4 (b) and (c) display the processed unwrapped phase and coherence values in the radar coordinate system, accounting for shadow and layover decorrelation using

https://doi.org/10.5194/isprs-annals-X-G-2025-11-2025

GAMMA software (Werner et al., 2000). A coherence threshold of 0.5 was applied to mask unstable pixels.

Figure 5 illustrates the reconstruction process for the masked patches of the interferogram in the test region. Despite the differences between training and testing data, the performance of the model remains robust, demonstrating adaptability to different topographic environments. This is critical for real-world applications, as InSAR data is often collected over diverse geographic areas, and a robust reconstruction method must handle variations in topographic conditions and decorrelation levels. The results for fringe reconnection and phase reconstruction remain consistent across different terrains, validating the effectiveness of the model in handling decorrelation over varying topographic features. The model demonstrates a correlation of 0.72–0.87 between the reconstructed and ground truth phases. The primary source of residual errors stems from phase-shifting areas, highlighting the role of fringe lines and the importance of further enhancing the fringe reconnection process.

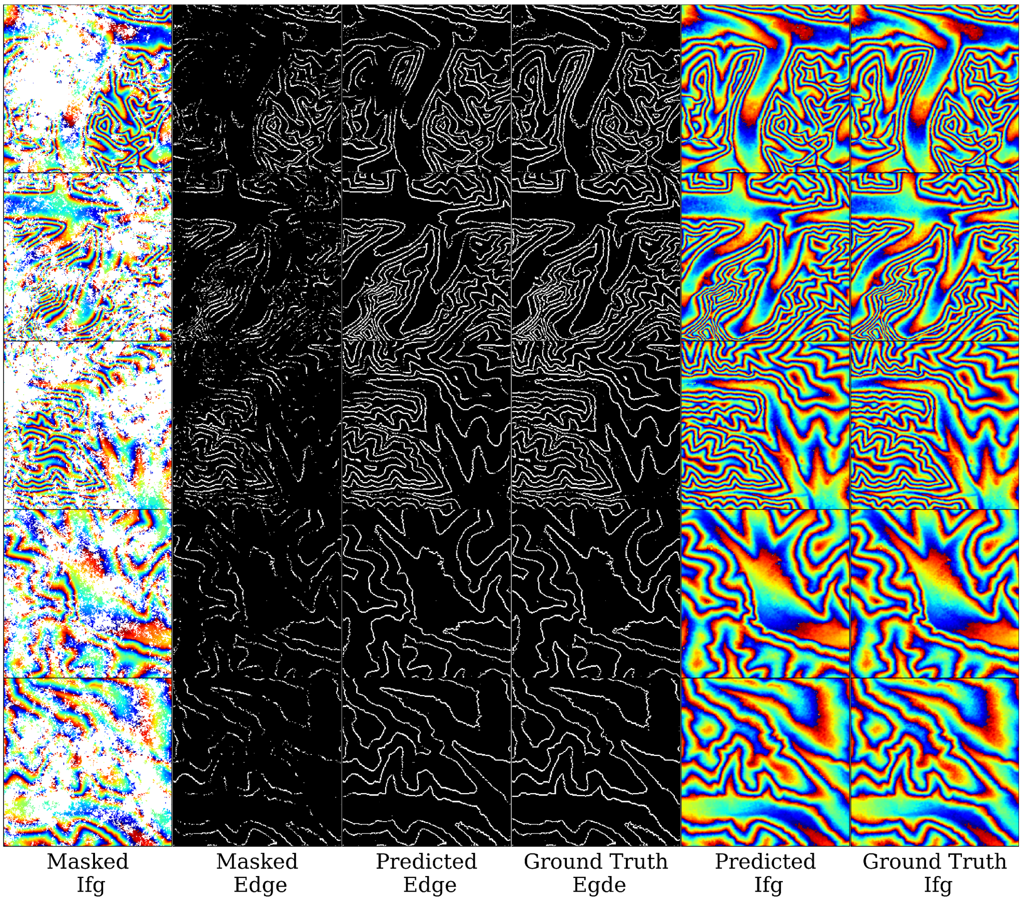

Figure 3. Results of reconstructing missing interferometric phase using a sample of the processed patches from the simulated InSAR dataset. The first column displays the masked interferograms. The second column presents the corresponding masked fringe lines. The third column illustrates the reconnected fringe lines. The fourth column shows the ground truth fringe lines. The fifth column provides the reconstructed interferograms. The sixth column contains the ground truth interferograms.

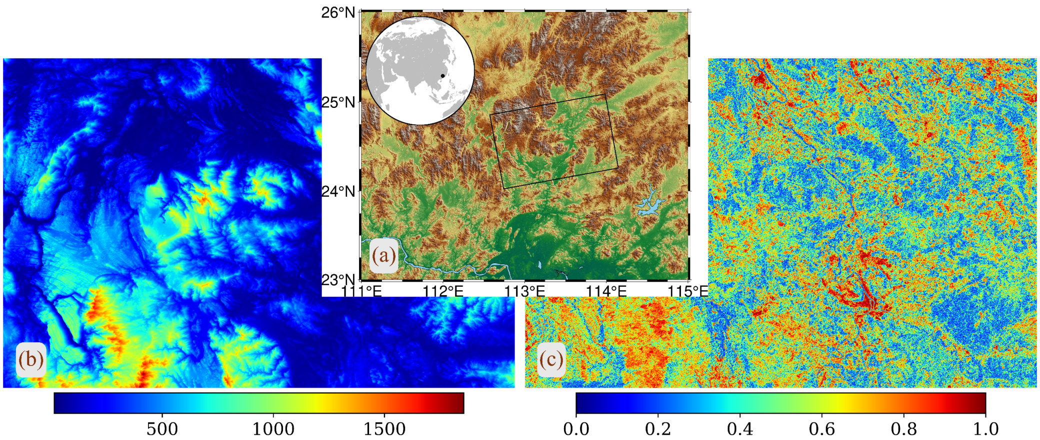

Figure 4. The real data used to test the networks. a) The Greater Bay Area (GBA) geographic location. The actual interferogram. c) The actual coherence.

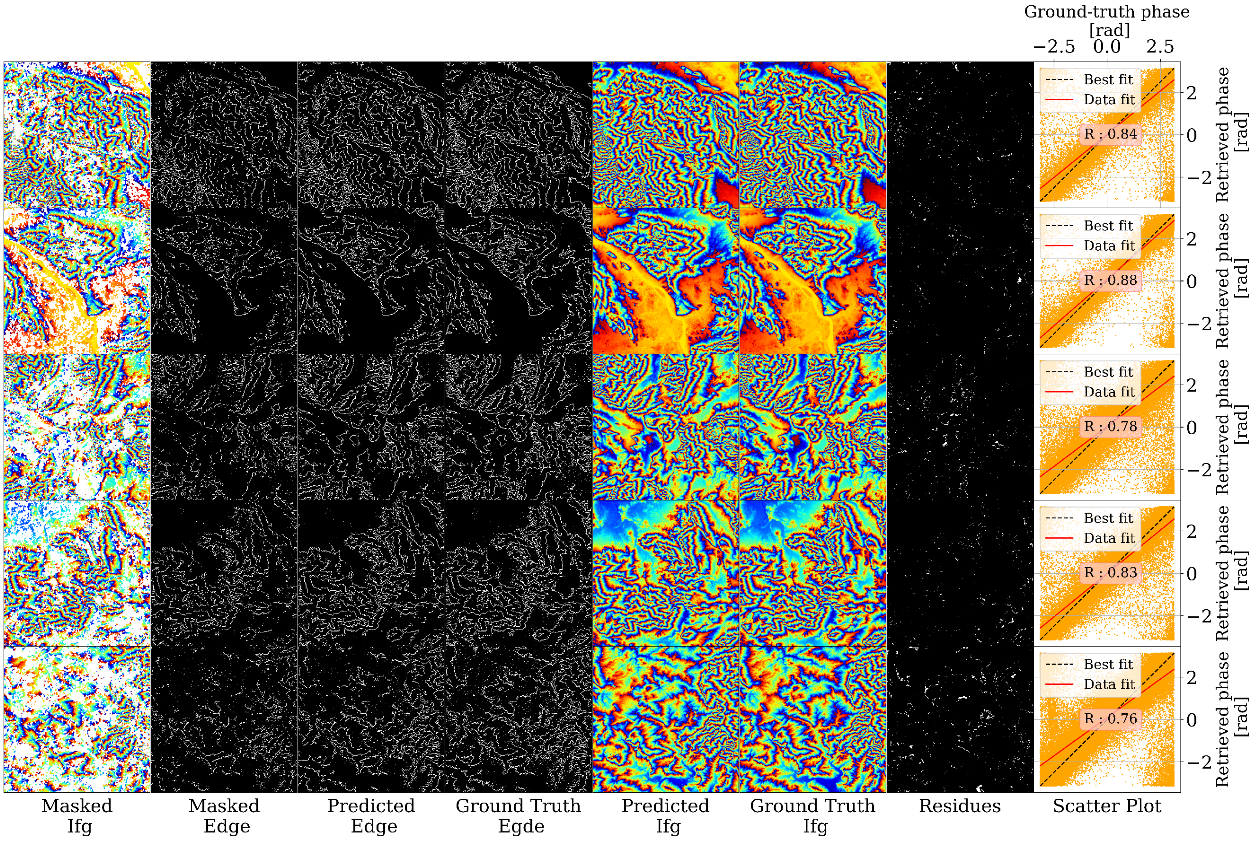

Figure 5. Results of reconstructing missing interferometric phase using a sample of processed patches with the corresponding decorrelation mask at a threshold of 0.5. The first column shows masked interferograms. The second column shows the corresponding masked fringe lines. The third column gives reconnected fringe lines. The fourth column contains the ground truth fringe lines. The fifth column gives corrected interferograms. The sixth column contains the ground truth interferograms. The seventh column contains the location of the residues. The eighth column contains the cross-plots of actual and predicted phases over the masked regions.

4. Summary and Conclusions

This paper presents a two-stage GAN-based framework for reconstructing interferometric phases over decorrelated regions. The first stage addresses the reconnection of fragmented phase fringes, while the second stage reconstructs the phase in masked regions, using the reconnected fringes as contextual information. The model was trained and tested on data from two areas in China, demonstrating its ability to generalize across different terrains with similar topographic complexities.

The experiment results indicate that the two-stage GAN framework outperforms single-stage reconstruction methods which use the mask as the conditional map, providing both quantitative and qualitative improvements in phase continuity and reconstruction accuracy. The model effectively mitigates decorrelation effects and achieves smoother phase transitions across masked regions. These enhancements are reflected in low error rates and high similarity metrics in both training, validation, and test datasets. Furthermore, the strong performance of the model in the test region highlights its potential for generalization to new, unseen geographic areas.

However, several challenges still remain, including instability during training and the high computational demands associated with both training and inference. The performance of the model in areas with extreme decorrelation may require further refinement, possibly through enhancements to the FRN. Additionally, incorporating transfer learning techniques could improve the ability to handle large-scale deformation and fine-grained noise.

In summary, the proposed two-stage GAN framework offers a promising solution for phase reconstruction in InSAR applications. It enables more accurate and reliable phase reconstructions over decorrelated regions. These advancements will enhance the monitoring and analysis of ground terrain in densely vegetated areas and natural hazards like earthquakes, landslides, and volcanic activity.

Acknowledgements

The research was jointly supported by the Research Grants Council (RGC) of the Hong Kong Special Administrative Region (Grants No. 152318/22, 152344/23), the National Natural Science Foundation of China (Grants No. 42330717), and the University Grants Council of the Hong Kong Polytechnic University (Grants No. P0045896). All the experiments were conducted using a high-performance computer in the Geohazard Lab provided by the Hong Kong Polytechnic University (PolyU).

References

Abdallah, M., Ding, X., Younis, S., Wu, S., 2025. A novel lightweight 3D CNN for accurate deformation time series retrieval in MT-InSAR. *Science of Remote Sensing*, 11, 100206. https://doi.org/10.1016/j.srs.2025.100206

Abdallah, M., Wu, S., Tayeb, S., Ding, X., 2024a. A New Approach for Interferometric Phase Reconstruction over

Decorrelated Regions with Deep Learning, in: IEEE International Conference on Signal, Information and Data Processing. Zhuhai.

Abdallah, M., Younis, S., Wu, S., Ding, X., 2024b. Automated deformation detection and interpretation using InSAR data and a multi-task ViT model. *International Journal of Applied Earth Observation and Geoinformation*, 128, 103758. https://doi.org/10.1016/j.jag.2024.103758

Chen, Y., Bruzzone, L., Jiang, L., Sun, Q., 2021. ARU-Net: Reduction of Atmospheric Phase Screen in SAR Interferometry Using Attention-Based Deep Residual U-Net. *IEEE Transactions on Geoscience and Remote Sensing*, 59, 5780–5793. https://doi.org/10.1109/TGRS.2020.3021765

Fang, Q., Xia, H., Song, Q., Zhang, M., Guo, R., Montresor, S., Picart, P., 2022. Speckle denoising based on deep learning via a conditional generative adversarial network in digital holographic interferometry. *Optics express.*,. https://doi.org/10.1364/OE.459213

Gavas, R.D., Ghosh, S.K., Pal, A., 2023. Enhanced Goldstein Filter for Interferometric Phase Denoising Using 2-D Variational Mode Decomposition. *IEEE Open Journal of Instrumentation and Measurement*, 2, 1–8. https://doi.org/10.1109/ojim.2023.3303948

Goldstein, R.M., Werner, C.L., 1998. Radar interferogram filtering for geophysical applications. *Geophysical Research Letters*, 25, 4035–4038. https://doi.org/10.1029/1998GL900033

Goodfellow, I., Pouget-Abadie, J., Mirza, M., Xu, B., Warde-Farley, D., Ozair, S., Courville, A., Bengio, Y., 2014. Generative Adversarial Networks. *Communications of the ACM*, 63, 139–144. https://doi.org/10.1145/3422622

Hanssen, R.F., 2001. Radar interferometry: data interpretation and error analysis, 1st ed. Springer Science & Business Media.

Hippert-Ferrer, A., Yan, Y., Bolon, P., 2021. EM-EOF: Gap-Filling in Incomplete SAR Displacement Time Series. *IEEE Transactions on Geoscience and Remote Sensing*, 59, 5794–5811. https://doi.org/10.1109/TGRS.2020.3015087

Isola, P., Zhu, J.Y., Zhou, T., Efros, A.A., 2017. Image-to-image translation with conditional adversarial networks. *Proceedings - 30th IEEE Conference on Computer Vision and Pattern Recognition, CVPR 2017*, 2017-Janua, 5967–5976. https://doi.org/10.1109/CVPR.2017.632

Kingma, D.P., Ba, J.L., 2015. Adam: A method for stochastic optimization. *3rd International Conference on Learning Representations, ICLR 2015 - Conference Track Proceedings*, 1–15. https://doi.org/10.48550/arXiv.1412.6980

Le, M., Kayal, S., 2021. Revisiting Edge Detection in Convolutional Neural Networks. *Proceedings of the International Joint Conference on Neural Networks*, 2021-July. https://doi.org/10.1109/IJCNN52387.2021.9534039

Lee, H., Liu, J.G., 2001. Analysis of topographic decorrelation in SAR interferometry using ratio coherence imagery. *IEEE Transactions on Geoscience and Remote Sensing*, 39, 223–232. https://doi.org/10.1109/36.905230

Nazeri, K., Ng, E., Joseph, T., Qureshi, F.Z., Ebrahimi, M., 2019. EdgeConnect: Generative Image Inpainting with Adversarial Edge Learning.

Prebet, R., Yan, Y., Jauvin, M., Trouve, E., 2019. A Data-Adaptive EOF-Based Method for Displacement Signal Retrieval from InSAR Displacement Measurement Time Series for Decorrelating Targets. *IEEE Transactions on Geoscience and Remote Sensing*, 57, 5829–5852. https://doi.org/10.1109/TGRS.2019.2902719

Rongier, G., Rude, C.M., Herring, T., Pankratius, V., 2020. An attempt at improving atmospheric corrections in InSAR using cycle-consistent adversarial networks. *EarthArXiv*, 1–12.

Russakovsky, O., Deng, J., Su, H., Krause, J., Satheesh, S., Ma, S., Huang, Z., Karpathy, A., Khosla, A., Bernstein, M., Berg, A.C., Fei-Fei, L., 2015. ImageNet Large Scale Visual Recognition Challenge. *International Journal of Computer Vision*, 115, 211–252. https://doi.org/10.1007/s11263-015-0816-y

Simonyan, K., Zisserman, A., 2015. Very deep convolutional networks for large-scale image recognition. *3rd International Conference on Learning Representations, ICLR 2015 - Conference Track Proceedings*, 1–14. https://doi.org/10.48550/arXiv.1409.1556

Werner, C., Wegmüller, U., Strozzi, T., Wiesmann, A., 2000. GAMMA SAR and interferometric processing software. *European Space Agency, (Special Publication) ESA SP*, 211–219.

Wu, M.-C., Liu, J.G., Mason, P.J., 2013. Adaptive local kriging to retrieve slant-range surface motion maps of the Wenchuan earthquake. *International Journal of Remote Sensing*, 34, 7589–7606. https://doi.org/10.1080/01431161.2013.822600

Zebker, H.A., Villasenor, J., 1992. Decorrelation in interferometric radar echoes. *IEEE Transactions on geoscience and remote sensing*, 30, 950–959.

Zhang, Q., Wang, T., Pei, Y., Shi, X., 2021. Selective Kernel Res-Attention UNet: Deep Learning for Generating Decorrelation Mask with Applications to TanDEM-X Interferograms. *IEEE Journal of Selected Topics in Applied Earth Observations and Remote Sensing*, 14, 8537–8551. https://doi.org/10.1109/JSTARS.2021.3105703

Zhou, L., Yu, H., Pascazio, V., Xing, M., 2022. PU-GAN: A One-Step 2-D InSAR Phase Unwrapping Based on Conditional Generative Adversarial Network. *IEEE Transactions on Geoscience and Remote Sensing*, 60, 1–10. https://doi.org/10.1109/TGRS.2022.3145342

Zhou, Z., Sun, X., Yang, F., Wang, Z., Goldsbury, R., Cheng, I., 2024. GANInSAR: Deep Generative Modeling for Large-Scale InSAR Signal Simulation. *IEEE Journal of Selected Topics in Applied Earth Observations and Remote Sensing*, 17, 5303–5316. https://doi.org/10.1109/JSTARS.2024.3361444